Electrical Power and Energy Systems 119 (2020) 105888

Contents lists available at ScienceDirect

Electrical Power and Energy Systems

journal homepage: www.elsevier.com/locate/ijepes

Kung's component extraction in power system fault location

Izudin Džafić[a,1], Rabih A. Jabr[b,*], Naida Fetić[c,1]

[a] University of Sarajevo, Faculty of Electrical Engineering, Zmaja od Bosne bb, 71000 Sarajevo, Bosnia and Herzegovina
[b] Department of Electrical & Computer Engineering, American University of Beirut, P.O. Box 11-0236, Riad El- Solh/Beirut 1107 2020, Lebanon
[c] International University of Sarajevo, Hrasnička, cesta 15, 71210 Sarajevo, Bosnia and Herzegovina

ARTICLE INFO

Keywords:
Fault feature extraction
Full-cycle Fourier algorithm
Kung's method
Nonlinear least-squares method

ABSTRACT

This paper presents a method for the accurate estimation of phasors in fault location applications. One of the essential tasks of power system digital relays is to decrease the consequences that follow faults by fast detection and localization. A fault signal (current and voltage) is typically composed of the fundamental component in addition to a damped DC signal, together with damped harmonics and inter-harmonics. A significant challenge in impedance-based fault analysis is the accurate estimation of the fundamental frequency component. While different variations of the Fourier-based algorithm are the most commonly used in the estimation of the fundamental component, their accuracy tends to be sufficient for protection relaying schemes but not for fault location. This paper proposes a novel fault feature extraction method that is highly accurate; it combines Kung's method for signal decomposition followed by a nonlinear least-squares estimation. The proposed technique has been successfully evaluated in the context of a fault location method; the numerical tests show that the proposed two-stage approach can accurately estimate phasor information in the presence of transients and noise.

1. Introduction

The electrical power system has an essential role in society, where life without a constant and reliable supply of electricity is unimaginable. It is therefore of high importance to restore power supply after a fault occurs with minimum interruption, via fast fault detection and localization. The occurrence of a fault in a typically nonlinear power network gives rise to transient signals (current and voltage) each formed by the fundamental frequency component, a decaying DC component, decaying harmonics (damped sinusoids at integer multiples, higher than one, of the fundamental power system frequency), and decaying inter-harmonics (damped sinusoids not at integer multiples of the fundamental frequency). The spreading of nonlinear loads and power electronic equipment in today's networks has increased harmonic and inter-harmonic pollution [1,2]. Damped harmonics and inter-harmonics have been observed in the transient signals during the ground fault in ungrounded networks (due to the earth capacitance) and distribution systems with compensated grounding (utilizing Peterson coil) [3,4]. Series compensated systems give rise to fault currents and voltages containing transients at sub-synchronous frequencies, in addition to higher-order harmonics and decaying inter-harmonics [4]. The methods for locating faults are well documented in [5]; the impedance-based methods typically make use either of the measured current and voltage at one end of the transmission line, or of two-end synchronized/unsynchronized measurements [6,7]. The estimation of the phasor voltages and currents during the fault is the first step in impedance-based fault location; in fact, the accuracy of the impedance-based methods hinges on the quality of the estimated phasors. The estimation of the fundamental component requires an algorithm that operates accurately against the undesired effects of the transient components after the occurrence of the fault.

1.1. Related work

The Discrete Fourier Transform (DFT) technique is practically the most commonly used method for phasor estimation, based on signal measurement while the fault is on. The main advantage of DFT is the low computational cost; it is however challenged by the filtering of the DC component, which has been tackled using the mimic filter [8,9], adaptive measuring [10], and other techniques [11–14]. The variations of the DFT-based algorithm (also known as orthogonal components method) are generally commensurate with the real-time computing requirements for digital protective relay applications. The magnitude response of the full-period Fourier method shows that DFT-based algorithms entirely reject harmonics [5]; however the use of power electronic equipment and compensated grounding give rise to damped

* Corresponding author.
E-mail addresses: idzafic@ieee.org (I. Džafić), rabih.jabr@aub.edu.lb (R.A. Jabr), nfetic@ius.edu.ba (N. Fetić).
[1] The work of I. Džafić and N. Fetić was supported by Siemens Energy Automation, Nuremberg, Germany.

https://doi.org/10.1016/j.ijepes.2020.105888
Received 4 September 2019; Received in revised form 12 December 2019; Accepted 27 January 2020
Available online 09 February 2020
0142-0615/ © 2020 Elsevier Ltd. All rights reserved.

inter-harmonics [2–4], i.e., damped sinusoids that are not integer multiples of the fundamental frequency and are therefore not wholly rejected.

Refs. [15,16] report that DFT-based algorithms have difficulty in handling slowly varying signals under dynamic conditions, and this problem has been approached via hybrid DFT techniques and the Prony method. The Prony method has also been employed for fault location in series-compensated lines, where the series capacitor gives rise to considerable sub-synchronous frequency components that are not sufficiently damped within the typical fault clearing time [4,17]. In the power systems literature, the Prony method is well known for its use in transient stability oscillations monitoring [18], and has been more recently proposed for synchro-phasor estimation from a one-cycle time window data [19]; Ref. [19] concludes that the Prony estimates are an improvement over Fourier under oscillation conditions, with measurements over a very short duration window. It is known however that the performance of the basic Prony method can quickly degrade with noise [20]; the proposed solutions in this case center around changing the sampling interval [21,22] and adaptive sampling schemes [23]. As an alternative methodology, the wavelet transform has been employed for power system frequency and phasor estimation [24,25]; despite its promising performance, the use of wavelets has not reached commercial applications.

1.2. Technical contribution

This paper proposes the use of Kung's method [26,27] for extracting phasor information under fault conditions, motivated by previous work that reported its superior accuracy to Prony's method [28–30]. However, Kung's method necessitates the use of Singular Value Decomposition (SVD), which is costly to calculate, while the conventional Prony least-squares method does not [31]. The improvement in accuracy at the expense of speed is worthwhile, as the application of Kung's method is targeted towards fault location which is not a real-time function. To further improve the estimation from Kung's method, the extracted phasor is used to initialize a Gauss-Newton least-squares estimator [32]; numerical experience shows that this two-stage solution procedure has a significant improvement on the estimation accuracy. The simulation results demonstrate that the suggested technique is highly accurate for phasor extraction in the presence of noise and analog to digital conversion error; in addition, it has significant benefits on synchronized measurement technology-based fault location [33].

1.3. Paper structure

The rest of this paper is organized as follows: Section 2 outlines the proposed technique and introduces the methods used for the identification of the fault signal components, while Section 3 details some practical implementation details. Numerical results are presented in Section 4; they show the superiority of the proposed method in comparison with an orthogonal components method [10,5] both on synthetically generated signals, and when employed for fault location on a practical transmission line in Bosnia. General conclusions are drawn in Section 5.

2. Component extraction methods

Noise significantly affects the feature extraction and may lead to the wrong diagnosis. The phasor estimator has to determine the amplitude and phase of the fundamental component from the noisy signal; the fundamental frequency is commonly obtained from the pre-fault data. Signal analysis tools that operate on analog inputs are limited by the finite resolution of the Analog to Digital Converters (ADCs) and the imperfections of electronic components [34]. The resolution of the ADC is characterized by the number of bits in the digital result and the input signal range. There are ADC converters with various resolutions of 4, 8, 10, 12, 14, 16, and 24 bits [35], while the input range is defined according to the analog input signal. Common ADC resolutions found on the market for power quality measurement are 12 and 14 bits. The first step in analyzing the fault signal is calculating the number of signal components. The transient signal typically includes a large number of components, which makes it necessary to estimate the model order as an input to the decomposition technique. In practice, a filter is applied to the input data so that all harmonic/inter-harmonic frequencies above 250 Hz are attenuated; the dominant components in the transient signal are the fundamental frequency component, the DC decaying term, and a few damped harmonic/inter-harmonic components having frequencies close to the power system frequency.

The rest of this section discusses three different component extraction methods: the full-cycle Fourier algorithm in Section 2.1, Prony's method in Section 2.2, and Kung's method in Section 2.3. The paper proposes a two-stage procedure comprising Kung's method followed by nonlinear least-squares estimation to obtain highly accurate phasor extraction results; this is reported in Section 2.4.

2.1. Full-cycle Fourier algorithm with decaying DC component

Orthogonal components (OC) or DFT-based methods are currently employed in practical digital protective relays. OC methods feature fast execution time as required for online applications, and accuracy sufficient for protection relaying; most employ the full-cycle Fourier algorithm, with special provisions for eliminating the decaying DC component [8–14].

Fig. 1 shows the magnitude response for the full-period Fourier algorithm used in the OC method. The figure reveals that the harmonic components (sinusoids at integer multiples, higher than one, of the fundamental frequency) are eliminated, while the inter-harmonics (sinusoids not at integer multiples of the fundamental frequency) are multiplied by a positive nonzero value less than one. For instance, if the fundamental frequency is 50 Hz, the inter-harmonics whose frequencies are around the mid of the interval between 50 Hz and 100 Hz are not rejected by the Fourier algorithm.

In the interest of speed, some variations of the OC method are designed to make use only of half a cycle of data [36,37]. Once the DC decaying component is eliminated, the Fourier algorithm effectively eliminates harmonics. For comparative analysis, this paper employs the full-cycle recursive Fourier algorithm in [10], which features two corrective functions for thorough rejection of the DC signal component. The details of the implementation are available in Section 4.3.2 of [5], and Matlab code is also provided in [5] for accurate replication of the results.

2.2. Prony least-squares method

The Prony method is a technique for the exponential fitting of time series data; it allows extracting the magnitude, angle, damping factor,

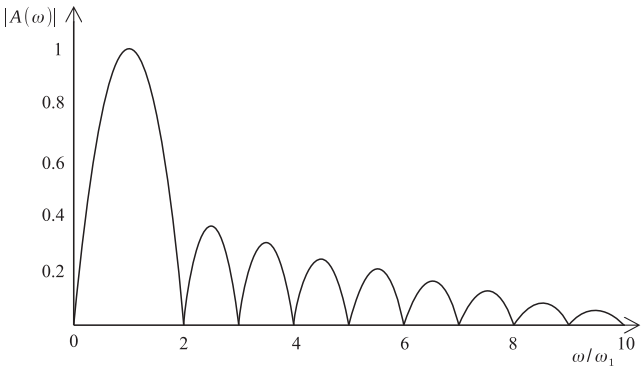

Fig. 1. Frequency characteristic of the OC method.

and frequency for each component (or mode) in the transient signal. However, Prony analysis is known to suffer from ill-conditioning with the increasing number of exponential terms, leading to errors in the root-finding computation [27]. The Prony least-squares method is a variation on the Prony method; it makes use of the least-squares estimation of the parameters of the Prony model to filter out noise.

Consider a typical power system response signal with a total number of modes p (1), which include the DC decaying component ($f_0 = 0$) and the fundamental component ($\tau_1 = 0$):

$$y(t) = \sum_{i=0}^{p-1} A_i e^{\tau_i t} \cos(2\pi f_i t + \phi_i) \tag{1}$$

Let $t = nT$, where T is a sampling period. The samples of $y(t)$ in the frequency domain could be written as:

$$y[n] = \sum_{i=0}^{p-1} C_i \lambda_i^n, \; n = 0, 1, 2...,N-1 \tag{2}$$

where C_i is a complex amplitude and $\lambda_i = e^{(\tau_i + 2j\pi f_i)t}$ is a complex frequency. Prony's method consists of three successive steps [1,18]: (i) computing the coefficients of the linear prediction model, (ii) finding the roots of the characteristic polynomial, and (iii) deducing the modal frequencies (that yield τ_i and f_i) together with the amplitude and phase of each mode (A_i and ϕ_i). Prony analysis starts with the following standard linear prediction equation:

$$\sum_{i=0}^{p-1} y_{k-p+i} a_i = -y_k \tag{3}$$

where $k = p, p+1, ...,2p-1$ and a is a vector of lag coefficients that contains the exponential parameters information. A matrix representation of the signal at various sample times can be formed by sequentially repeating the linear prediction of y_k:

$$\begin{bmatrix} y_0 & y_1 & \cdots & y_{p-1} \\ y_1 & y_2 & \cdots & y_p \\ \vdots & \vdots & & \vdots \\ y_{p-1} & y_p & \cdots & y_{2p-2} \end{bmatrix} \begin{bmatrix} a_0 \\ a_2 \\ \vdots \\ a_{p-1} \end{bmatrix} = - \begin{bmatrix} y_p \\ y_{p+1} \\ \vdots \\ y_{2p-1} \end{bmatrix} \tag{4}$$

Eq. (4) is written in matrix form as:

$$H \cdot a = -h \tag{5}$$

In order to reduce the effect of noise, the number of rows in (4) is chosen to be greater than the prediction model order p; for instance, [38] recommends a number of samples three times larger than the order of the model. In this case, H is an $(N-p) \times p$ matrix of sampled data, a is a column vector of size p, and y is a column vector of size $(N-p)$; the constituent elements are given by:

$$\begin{bmatrix} y_0 & y_1 & \cdots & y_{p-1} \\ y_1 & y_2 & \cdots & y_p \\ \vdots & \vdots & \vdots & \vdots \\ y_{N-p-1} & y_{N-p} & \cdots & y_{N-2} \end{bmatrix} \begin{bmatrix} a_0 \\ a_2 \\ \vdots \\ a_{p-1} \end{bmatrix} = - \begin{bmatrix} y_p \\ y_{p+1} \\ \vdots \\ y_{N-1} \end{bmatrix} \tag{6}$$

The system in (6) is over-determined; its solution is therefore obtained by solving the minimum error problem:

$$\min_a \; \|Ha + h\|^2 \tag{7}$$

The minimum norm solution to this minimum error problem can be written in terms of the pseudo-inverse H^+:

$$a = -H^+ h \tag{8}$$

In the conventional linear prediction models, the pseudo-inverse accounts for noise on the right-hand side of (6) and the solution is obtained via the normal equations approach [31]. An improvement in the estimation could be obtained using the total least-squares method, which accounts for noise in both the coefficient matrix and right-hand side of (6); this, however, requires using the more computationally expensive SVD [31,39]. Once the linear prediction coefficients in a are estimated, the eigenvalues are then recovered as the roots of the characteristic polynomial:

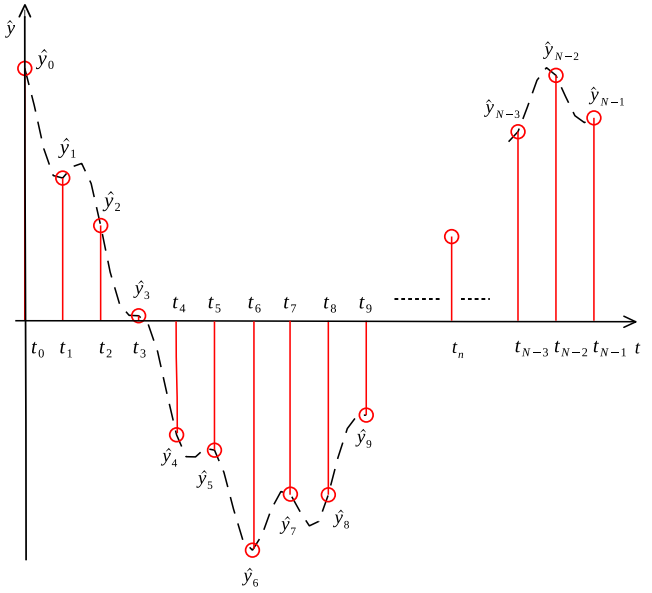

Fig. 2. Measured signal.

$$\lambda^p - a_0\lambda^{p-1} - ... - a_{p-2}\lambda - a_{p-1} = (\lambda - \hat{\lambda}_0)(\lambda - \hat{\lambda}_1)...(\lambda - \hat{\lambda}_{p-1}) = 0 \tag{9}$$

The damping factor and frequency of the signal are extracted from (10) and (11):

$$\tau_i = \frac{\text{real}(\lambda_i)}{T} \tag{10}$$

$$f_i = \text{imag}(\lambda_i) 2\pi T \tag{11}$$

In the last step, the complex amplitudes are obtained from:

$$y = \Lambda C \tag{12}$$

where

$$y = [y_0 \;\; y_1 \;\; \cdots \;\; y_{N-1}]^T \tag{13}$$

$$\Lambda = \begin{bmatrix} 1 & 1 & \cdots & 1 \\ \lambda_0^1 & \lambda_1^1 & \cdots & \lambda_{p-1}^1 \\ \vdots & \vdots & \vdots & \vdots \\ \lambda_0^{N-1} & \lambda_1^{N-1} & \cdots & \lambda_{p-1}^{N-1} \end{bmatrix} \tag{14}$$

$$C = [C_0 \;\; C_1 \;\; \cdots \;\; C_{p-1}]^T \tag{15}$$

The vector C in (12) is then solved for using the least-squares method; from this solution, the magnitude A_i and phase angle ϕ_i are then computed. The amplitudes for the modal components with nonzero frequency are given by:

$$A_i = 2 \cdot |C_i| \tag{16}$$

while for the decaying DC component the amplitude is:

$$A_0 = |C_0| \tag{17}$$

The phase angles are finally obtained from:

$$\phi_i = \angle C_i \tag{18}$$

2.3. Kung's method

Another method for exponential fitting is Kung's method [26].

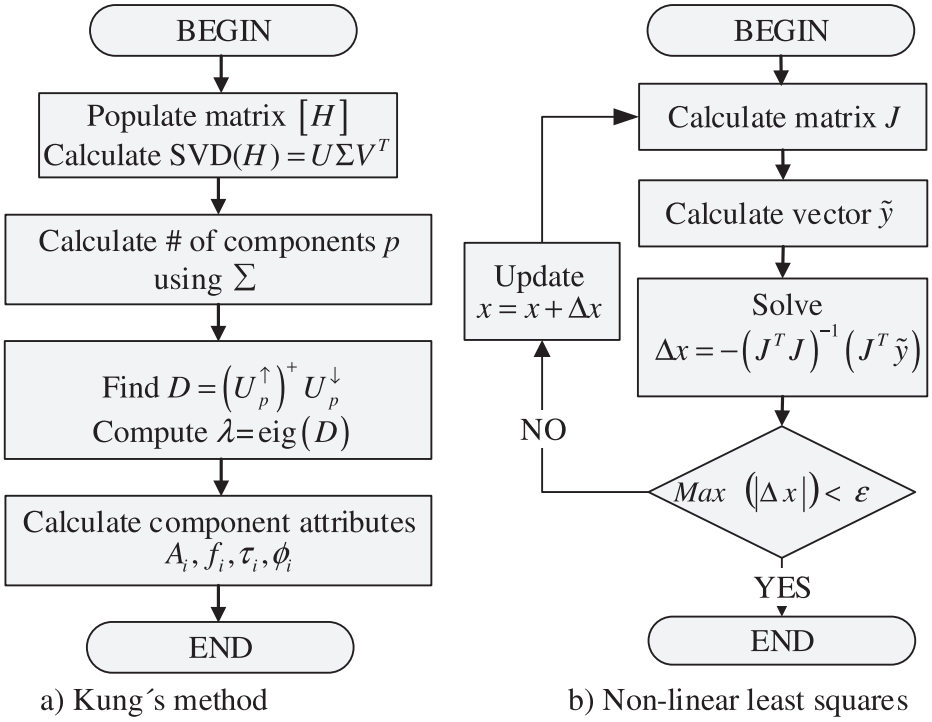

Fig. 3. (a) Kung's method and (b) nonlinear least-squares.

According to [28–30], Kung's method is more accurate than the Prony least-squares solution in the presence of noise; a more recent Ph.D. thesis reported a numerical comparison between Kung's method and Prony least-squares that quantifies the numerical superiority of Kung's method in terms of reduced eigenvalue error (c.f. Fig. 2.7 in [27]). However, the use of SVD in Kung's method is inevitable, which makes Kung's method less computationally efficient than Prony's method that uses the normal equations least-squares solution.

Kung's method [26,27] is better at filtering noise as it estimates the signal poles using the left singular values of the Hankel matrix. The Hankel matrix of a signal $y[n]$, $n = 0, 1, \cdots N-1$ is built as in (6). By judiciously truncating the SVD of the data matrix, the pole information is extracted from the signal subspace basis that has a dimension equal to the number of exponential terms in the signal:

$$H = U_p \Sigma_p V_p^T \tag{19}$$

where U_p, Σ_p, and V_p are the first p columns of the SVD matrices U, Σ, and V. The total number of modes p in the signal model is computed from the rank of the matrix Σ, practically as shown in Algorithm 1. The algorithm checks the ratio of the absolute values of the consecutive singular values and identifies a substantial drop; the number of components is equal to the number of singular values before the drop. Using the Vandermonde decomposition [29,40–42], the poles can be then obtained by calculating the eigenvalues of the matrix D:

$$D = (U_p^{\uparrow})^{+} U_p^{\downarrow} \tag{20}$$

where $(U_p^{\uparrow})^{+}$ represents the pseudo inverse of $U_p^{\uparrow}$, calculated using the SVD method. The matrix $U_p^{\downarrow}$ is obtained by removing the first row of the left singular values matrix U_p, and $U_p^{\uparrow}$ is obtained by removing the last row of U_p. The signal pole estimates are then computed as:

$$\lambda = \text{eig}(D) \tag{21}$$

and the signal components' damping coefficient τ_i and frequency f_i are deduced using (10) and (11). The complex amplitudes C_i (15) are then obtained as in Prony's method, i.e. by fitting (12) to the data of the estimated signal poles in (14) and the data samples in (13) [42,43]; the amplitude and phase parameters are subsequently deduced via (16)–(18). Kung's algorithm is summarized in Fig. 3a.

Algorithm 1. Detection of the number of components $S = \Sigma$

```
ratio = 100; %typical value
for p = 2:m
  if abs(S(p − 1,p − 1)/S(p,p)) > ratio
    return p − 1;
end
return m;
```

2.4. Nonlinear least-squares

The nonlinear least-squares (LS) method is an alternative to the Prony and Kung's methods; it is a maximum likelihood method, i.e., it aims to maximize the likelihood of the estimated vector from noisy measurements [27]. The maximum likelihood problem is equivalent to a nonlinear LS problem, which could be efficiently solved using the Gauss-Newton method [32]. The nonlinear LS method starts from an initial estimate, and iteratively moves towards a better solution; it is well known that without a reasonable initial estimate of the vector of parameters, the optimization can lead to an unacceptable solution. The Prony-type methods discussed in Sections 2.2 and 2.3 do not, however, require an initial solution, which makes them an ideal source for the initial estimates needed by the Gauss-Newton method [27]. The overall proposed method for phasor extraction employs Kung's method to initialize the nonlinear LS optimization routine. The development of the Gauss-Newton method is detailed below.

Fig. 2 depicts a real-valued nonlinear function which consists of n evenly spaced samples at t_n; its model can be expressed as:

$$y(\boldsymbol{x}, t_n) = \sum_{i=0}^{p-1} A_i e^{\tau_i t_n} \cos(2\pi f_i t_n + \phi_i) \tag{22}$$

where p is the number of signal components in the signal, and $\boldsymbol{x}$ is composed of sub-vectors $\boldsymbol{s}_0 = [A_0 \;\; \tau_0]$ for the decaying DC component, $\boldsymbol{s}_1 = [A_1 \;\; \phi_1]$ for the fundamental AC component, and $\boldsymbol{s}_i = [A_i \;\; f_i \;\; \tau_i \;\; \phi_i]$

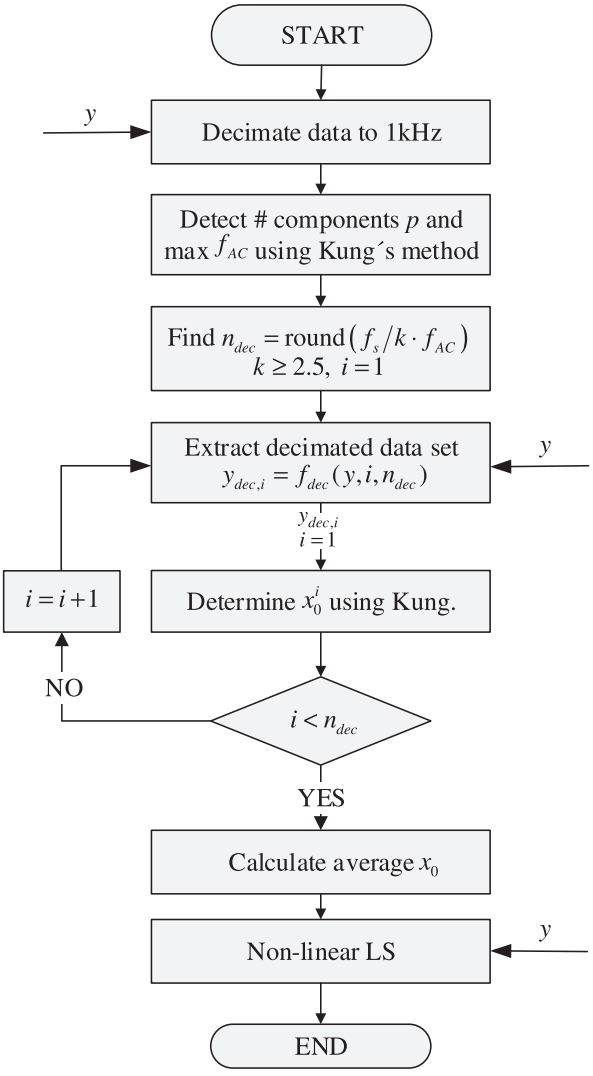

Fig. 4. The proposed method.

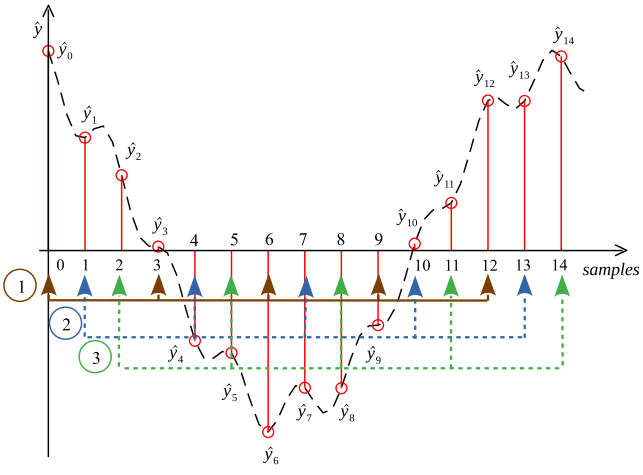

Fig. 5. Example of signal decimation for averaging with $n_{dec} = 3$.

that holds the unknown variables for the i-th component ($i = 2, \ldots, p-1$):

$$\boldsymbol{x} = [\boldsymbol{s}_0, \boldsymbol{s}_1, \ldots, \boldsymbol{s}_{p-1}]^T \tag{23}$$

The solution to the unconstrained minimization problem in (24) gives

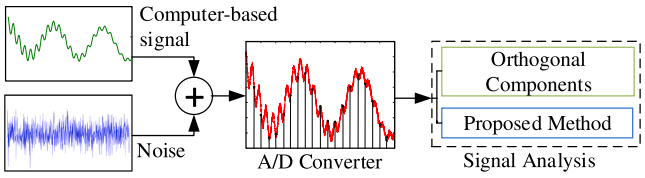

Fig. 6. Phasor extraction.

Table 1
Parameter values of the test signal components.

Attribute	Comp. #1	Comp. #2	Comp. #3	MC Variation
A	0.5	20	0.3	± 60%
τ	− 30	0	− 30	± 60%
f [Hz]	f_{AC}	50.5	0.0	0%
ϕ [deg]	30.0°	22.5°	0.0°	± 60%

the vector $\boldsymbol{x}$ (i.e. amplitude A_i, the damping coefficient τ_i, the frequency f_i, and the phase ϕ_i of the different modes):

$$\min_{\boldsymbol{x}} F(\boldsymbol{x}) = \frac{1}{2} \sum_{n=0}^{N-1} (\tilde{y}_n(\boldsymbol{x}))^2 \tag{24}$$

In (24), $\tilde{y}_n(\boldsymbol{x})$ represents the difference between the value from the measurement model (22) and the actual measured value at t_n:

$$\tilde{y}_n(\boldsymbol{x}) = y(\boldsymbol{x}, t_n) - \hat{y}_n \tag{25}$$

where $\hat{y}_n$ is the measured data value. The solution to this problem starts from an initial guess for the unknown variables (which is the solution by Kung's method, $\boldsymbol{x}^{(0)}$). At iteration k, $\tilde{y}_n(\boldsymbol{x})$ is linearized around the current guess $\boldsymbol{x}^{(k)}$:

$$\tilde{y}_n(\boldsymbol{x}) \simeq \tilde{y}_n(\boldsymbol{x}^{(k)}) + \nabla \tilde{y}_n(\boldsymbol{x}^{(k)})^T (\boldsymbol{x} - \boldsymbol{x}^{(k)}) \tag{26}$$

Substituting (26) in (24) and rearranging terms gives [32]:

$$\min_{\Delta \boldsymbol{x}^{(k)}} \| J(\boldsymbol{x}^{(k)}) \Delta \boldsymbol{x}^{(k)} + \tilde{y}(\boldsymbol{x}^{(k)}) \|_2^2 \tag{27}$$

where $J(\boldsymbol{x}^{(k)})$ is the Jacobian matrix (28) and $\Delta \boldsymbol{x}^{(k)}$ is the step size found by solving the normal equations for the linear least-squares problem (29):

$$J = \begin{bmatrix} \frac{\partial \tilde{y}_0}{\partial s_0(1)} & \frac{\partial \tilde{y}_0}{\partial s_0(2)} & \cdots & \frac{\partial \tilde{y}_0}{\partial s_{p-1}(1)} & \cdots & \frac{\partial \tilde{y}_0}{\partial s_{p-1}(4)} \\ \frac{\partial \tilde{y}_1}{\partial s_0(1)} & \frac{\partial \tilde{y}_1}{\partial s_0(2)} & \cdots & \frac{\partial \tilde{y}_1}{\partial s_{p-1}(1)} & \cdots & \frac{\partial \tilde{y}_1}{\partial s_{p-1}(4)} \\ \vdots & \vdots & \cdots & \vdots & \cdots & \vdots \\ \frac{\partial \tilde{y}_{N-1}}{\partial s_0(1)} & \frac{\partial \tilde{y}_{N-1}}{\partial s_0(2)} & \cdots & \frac{\partial \tilde{y}_{N-1}}{\partial s_{p-1}(1)} & \cdots & \frac{\partial \tilde{y}_{N-1}}{\partial s_{p-1}(4)} \end{bmatrix} \tag{28}$$

$$J(\boldsymbol{x}^{(k)})^T J(\boldsymbol{x}^{(k)}) \Delta \boldsymbol{x}^{(k)} = -J(\boldsymbol{x}^{(k)})^T \tilde{y}(\boldsymbol{x}^{(k)}) \tag{29}$$

To form the Jacobian (28), the following derivatives are employed:

$$\frac{\partial \tilde{y}_n}{\partial A_i} = e^{\tau_i t_n} \cos(2\pi f_i t_n + \phi_i) \tag{30}$$

$$\frac{\partial \tilde{y}_n}{\partial f_i} = -A_i 2\pi t_n e^{\tau_i t} \sin(2\pi f_i t_n + \phi_i) \tag{31}$$

$$\frac{\partial \tilde{y}_n}{\partial \tau_i} = A_i t_n e^{\tau_i t} \cos(2\pi f_i t_n + \phi_i) \tag{32}$$

$$\frac{\partial \tilde{y}_n}{\partial \phi_i} = -A_i e^{\tau_i t} \sin(2\pi f_i t_n + \phi_i) \tag{33}$$

Once $\Delta \boldsymbol{x}^{(k)}$ is computed, the new iterate is updated:

$$\boldsymbol{x}^{(k+1)} = \boldsymbol{x}^{(k)} + \Delta \boldsymbol{x}^{(k)} \tag{34}$$

and the procedure is repeated until $\| \Delta \boldsymbol{x}^{(k)} \| \leqslant \varepsilon$, where ε is a pre-specified tolerance. Fig. 3 summarizes the overall methodology of the

Table 2
Comparison of the proposed method with the orthogonal components method for different noise levels (1000 Monte-Carlo trials).

		Error [%]									
SNR	f_{AC}: n_{dec}:	80 Hz 30		98.7Hz 20		125.7Hz 18		185.4Hz 13		225.6Hz 11	
[dB]	Attrib.	PM	OC	PM	OC	PM	OC	PM	OC	PM	OC
20.00	A	0.001	0.402	0.01	1.79	0.02	1.90	0.03	2.59	0.02	1.13
	ϕ	0.002	3.099	0.04	3.57	0.07	7.76	0.08	2.97	0.08	1.82
16.99	A	0.002	0.374	0.03	1.81	0.04	1.93	0.05	2.61	0.05	1.12
	ϕ	0.028	3.088	0.07	3.58	0.13	7.84	0.14	3.00	0.13	1.81
15.23	A	0.003	0.399	0.09	1.79	0.10	1.92	0.10	2.62	0.10	1.11
	ϕ	0.064	3.091	0.16	3.62	0.20	7.81	0.23	3.01	0.24	1.79
13.98	A	0.004	0.414	0.10	1.82	0.12	1.94	0.12	2.63	0.13	1.13
	ϕ	0.108	2.993	0.25	3.56	0.29	7.79	0.33	2.98	0.36	1.78
13.01	A	0.003	0.208	0.11	1.78	0.13	1.90	0.15	2.62	0.16	1.12
	ϕ	0.185	2.921	0.32	3.58	0.39	7.74	0.42	2.99	0.43	1.81

Table 3
Range and improvement factor of the estimated parameters (1000 Monte-Carlo trials).

SNR	Attribute			Error [%]						
		f_{AC}	n_{dec}	Min		Max		Avg.		**IF**
[dB]		[Hz]		PM	OC	PM	OC	PM	OC	
20.00	A	80	30	0.00	0.02	0.01	1.88	0.001	0.402	**402.00**
	ϕ			0.00	1.10	0.02	8.96	0.002	3.099	**1549.5**
	A	98.7	20	0.00	0.32	0.26	6.39	0.01	1.79	**179.00**
	ϕ			0.00	0.00	0.76	20.44	0.04	3.57	**89.25**
	A	125.7	18	0.00	0.36	0.26	7.72	0.02	1.90	**95.00**
	ϕ			0.00	0.00	0.93	34.23	0.07	7.76	**110.86**
	A	185.4	13	0.00	0.48	0.33	9.74	0.03	2.59	**86.33**
	ϕ			0.00	0.00	0.79	15.80	0.08	2.97	**37.13**
	A	225.6	11	0.00	0.20	0.33	4.28	0.02	1.13	**56.50**
	ϕ			0.00	0.00	0.86	9.83	0.08	1.82	**22.75**
15.23	A	80	30	0.00	0.022	0.017	2.045	0.003	0.399	**133.00**
	ϕ			0.00	0.904	0.049	8.970	0.064	3.091	**48.30**
	A	98.7	20	0.00	0.32	1.64	6.70	0.09	1.79	**19.89**
	ϕ			0.00	0.00	0.24	19.76	0.16	3.62	**22.63**
	A	125.7	18	0.00	0.34	0.97	7.91	0.10	1.92	**19.20**
	ϕ			0.00	0.00	1.25	36.47	0.20	7.81	**39.05**
	A	185.4	13	0.00	0.37	0.81	10.88	0.10	2.62	**26.20**
	ϕ			0.00	0.00	1.21	15.93	0.23	3.01	**13.09**
	A	225.6	11	0.00	0.16	0.84	4.41	0.10	1.11	**11.10**
	ϕ			0.00	0.00	1.55	9.49	0.24	1.79	**7.46**
13.01	A	80	30	0.00	0.028	0.017	1.858	0.003	0.208	**69.33**
	ϕ			0.00	0.985	0.068	9.009	0.185	2.921	**15.79**
	A	98.7	20	0.00	0.16	1.16	6.82	0.11	1.78	**16.18**
	ϕ			0.00	0.00	1.65	20.64	0.32	3.58	**11.19**
	A	125.7	18	0.00	0.26	1.37	7.54	0.13	1.90	**14.62**
	ϕ			0.00	0.02	1.74	32.94	0.39	7.74	**19.25**
	A	185.4	13	0.00	0.41	1.31	9.90	0.15	2.62	**17.47**
	ϕ			0.00	0.00	2.47	17.01	0.42	2.99	**7.12**
	A	225.6	11	0.00	0.06	1.61	4.60	0.16	1.12	**7.00**
	ϕ			0.00	0.00	3.51	10.47	0.43	1.81	**4.21**

proposed phasor estimator, where the first flowchart gives the initial solution via Kung's method, and the second flowchart improves Kung's estimate using nonlinear LS.

3. Practical implementation details

Fig. 3 summarizes the two main building blocks of the proposed phasor extraction approach: Kung's method followed by nonlinear least-squares. The practical implementation details of the proposed method are given in Fig. 4, which features Kung's method (Fig. 3a) in two blocks and the nonlinear LS solution (Fig. 3b) in one block. While practical hardware implementations sample at a frequency f_s between 4 and 8 kHz, Prony-type algorithms produce accurate results with a sampling frequency that is 2 to 3 times the maximum modal frequency in the signal [1]. The sampled data is therefore first decimated to 1 kHz, and Kung's method is used to determine the number of components p

Table 4
Comparison of the proposed method with Kung's method for different noise levels (1000 Monte-Carlo trials).

		Error [%]							
	f_{AC}:	98.7 Hz		125.7 Hz		185.4 Hz		225.6 Hz	
SNR	n_{dec}:	20		18		13		11	
[dB]	Attr.	Kung's	PM	Kung's	PM	Kung's	PM	Kung's	PM
20.00	A	0.08	0.01	0.08	0.02	0.07	0.03	0.18	0.02
	ϕ	0.45	0.04	0.43	0.07	0.11	0.08	1.61	0.08
16.99	A	0.17	0.05	0.15	0.05	0.13	0.06	0.43	0.07
	ϕ	0.89	0.12	0.80	0.14	2.29	0.17	3.85	0.15
15.23	A	0.25	0.09	0.24	0.10	0.23	0.10	0.68	0.10
	ϕ	1.34	0.16	1.39	0.20	3.63	0.23	5.59	0.24
13.98	A	0.32	0.10	0.33	0.11	0.30	0.12	0.86	0.13
	ϕ	1.69	0.24	1.78	0.29	4.72	0.32	7.01	0.34
13.01	A	0.41	0.11	0.42	0.13	0.36	0.15	1.03	0.16
	ϕ	2.24	0.32	2.17	0.39	5.90	0.42	8.09	0.43

Table 5
Number of iterations and time results for Nonlinear Least-Squares (1000 Monte-Carlo Simulations, i5-7600 K, 16 GB RAM).

SNR			Num. of Iterations			Time [ms]		
[dB]	f_{AC}	n_{dec}	Min	Avg.	Max	Min	Avg.	Max
20.00	80	30	1	3.8	8	22.3	80.5	183.8
	98.7	20	1	3.2	7	21.5	70.9	162.5
	125.7	18	1	4.1	8	21.8	94.7	184.9
	185.4	13	2	5.8	10	43.8	135.9	234.3
	225.6	11	1	5.3	9	23.1	118.8	205.8
15.23	80	30	1	3.7	8	22.5	79.9	189.0
	98.7	20	1	3.2	7	21.7	75.0	154.9
	125.7	18	1	3.6	8	22.6	85.4	191.6
	185.4	13	2	5.9	10	42.8	131.3	231.1
	225.6	11	1	5.2	9	21.5	115.2	203.2
13.01	80	30	1	3.6	8	22.8	79.6	199.7
	98.7	20	1	2.9	7	22.4	68.9	163.1
	125.7	18	1	4.3	9	22.6	99.1	218.7
	185.4	13	1	6.1	10	21.8	143.6	234.8
	225.6	11	1	5.4	9	21.7	119.5	203.9

and the highest modal frequency; this is followed by computing the number of decimation stages n_{dec}. Fig. 5 shows an example of signal decimation with $n_{dec} = 3$, and the three corresponding sets of data points marked in brown, blue, and green. For the first extracted data series (corresponding to points sampled at positions 0, 3, 6, 9, and 12 in Fig. 5), Kung's method is used again to find the initial attributes of the modes (in $\boldsymbol{x}_0$). Once the phasor attributes are computed for all the decimated data sets, their averages are further improved via nonlinear least-squares and then reported as the final estimate of the phasor.

4. Numerical results

Fig. 6 illustrates how the numerical testing is carried out: starting with the generated signal at the output of the lowpass filter, add noise, and sample the resulting signal using the Analog-to-Digital converter. The phasor at the fundamental frequency is then extracted using one of two methods: the orthogonal components (OC) method described in Section 2.1, which is state-of-the-art adopted by the industry, and the proposed method (PM) as outlined in Fig. 4.

4.1. Simulation tests with frequency components having frequencies less than 250 Hz

The test signal is comprised of three components whose parameters are given in Table 1. The first component is the damped AC signal with a frequency f_{AC}, which will take the following values during testing: 80 Hz, 98.7 Hz, 125.7 Hz, 185.4 Hz, and 225.6 Hz; note that the values of f_{AC} are intentionally chosen to be non-integer multiples of the fundamental frequency. The second component is the AC signal set at a frequency slightly above 50 Hz, and the third component is the decaying DC term:

$$y_1 = 0.5e^{-30t}\cos(2\pi \cdot f_{AC} \cdot t + 30°) \tag{35}$$

$$y_2 = 20\cos(2\pi \cdot 50.5 \cdot t + 22.5°) \tag{36}$$

$$y_3 = 0.3e^{-30t} \tag{37}$$

Analog to digital conversion and noise both have an impact on the fault feature extraction methods. The numerical results consider an ADC with 16 bits and a range of ± 40; five different noise levels are considered with Signal-to-Noise Ratio (SNR) values of 20 dB, 16.99 dB, 15.23 dB, 13.98 dB, and 13.01 dB. The results in Table 2 report the percentage estimation errors of the phasor attributes (amplitude and phase angle) from PM and OC; each reported percentage estimation error value $\left(\frac{|\text{estimated value} - \text{true value}|}{\text{true value}} \times 100\right)$ in Table 2 has been averaged over 1000 Monte-Carlo (MC) trials of noise sampled from a uniform distribution having the specified maximum/minimum noise level; in addition, the true values of the attributes A, τ and ϕ for all the three components were randomly changed in the range ± 60% of the values listed in Table 1 and in Eqs. (35)–(37). The number of decimation levels n_{dec} for PM is obtained following the procedure in Fig. 4, with k around 2.5 and a sampling frequency $f_s = 6$ kHz; OC does not require a value for n_{dec} and uses the same sampling frequency. The results in Table 2 demonstrate that in terms of accuracy, the proposed method is superior to the Fourier-based approach with decaying DC component extraction. This is further illustrated in Table 3 that shows for both methods the minimum, maximum, and average values of the recorded errors over 1000 Monte-Carlo trials; the last column of this table shows a significant improvement factor $\left(\mathbf{IF} = \frac{\text{Avg. (OC)}}{\text{Avg. (PM)}}\right)$ of the PM relative to OC. Table 4 demonstrates the advantage of improving Kung's estimate of the phasor attributes via the nonlinear least-squares processing (discussed in Section 2.4); it shows that the average error over 1000 Monte-Carlo simulations when using Kung's method on its own is consistently higher as compared to using the proposed two-stage method.

Table 6
Parameter values of the test signal with four components.

Attribute	Comp. #1	Comp. #2	Comp. #3	Comp. #4	MC Variation
A	1.5	20	0.8	0.3	± 60%
τ	− 20	0	− 20	− 25	± 60%
f [Hz]	f_{AC}	50.5	0.0	f_4	0%, f_4 (250 − 400) Hz
ϕ [deg]	60.0°	22.5°	0.0°	25.0°	± 60%

Table 7
Comparison of the proposed method with the orthogonal components method for different noise levels and signals with four components (1000 Monte-Carlo trials).

		Error [%]									
SNR	f_{AC}: n_{dec}:	70 Hz 6		98.7Hz 6		125.7 Hz 6		185.4 Hz 6		225.6 Hz 6	
[dB]	Attr.	PM	OC	PM	OC	PM	OC	PM	OC	PM	OC
20.00	A	0.027	2.618	0.036	0.911	0.029	1.641	0.041	1.667	0.041	1.427
	ϕ	0.033	8.891	0.053	1.754	0.081	4.264	0.097	2.547	0.109	2.037
16.99	A	0.041	2.807	0.059	0.981	0.032	1.796	0.053	1.71	0.052	1.448
	ϕ	0.052	10.068	0.069	2.014	0.128	4.532	0.159	2.659	0.227	2.094
15.23	A	0.062	2.823	0.081	1.076	0.105	1.879	0.124	1.748	0.14	1.482
	ϕ	0.079	11.055	0.163	2.069	0.229	4.739	0.277	2.635	0.405	2.159
13.98	A	0.092	2.828	0.094	1.082	0.14	1.885	0.143	1.758	0.157	1.488
	ϕ	0.129	11.094	0.142	2.109	0.238	5.169	0.336	2.724	0.412	2.167
13.01	A	0.133	2.853	0.147	1.176	0.196	1.894	0.203	1.772	0.287	1.493
	ϕ	0.201	11.174	0.214	2.169	0.318	5.267	0.492	2.814	0.548	2.273

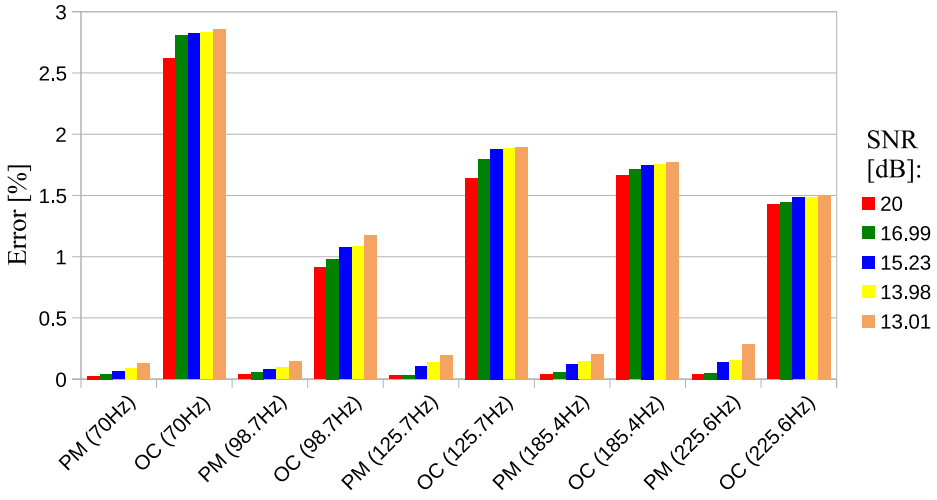

Fig. 7. Percentage estimation error of the amplitude A of the fundamental component.

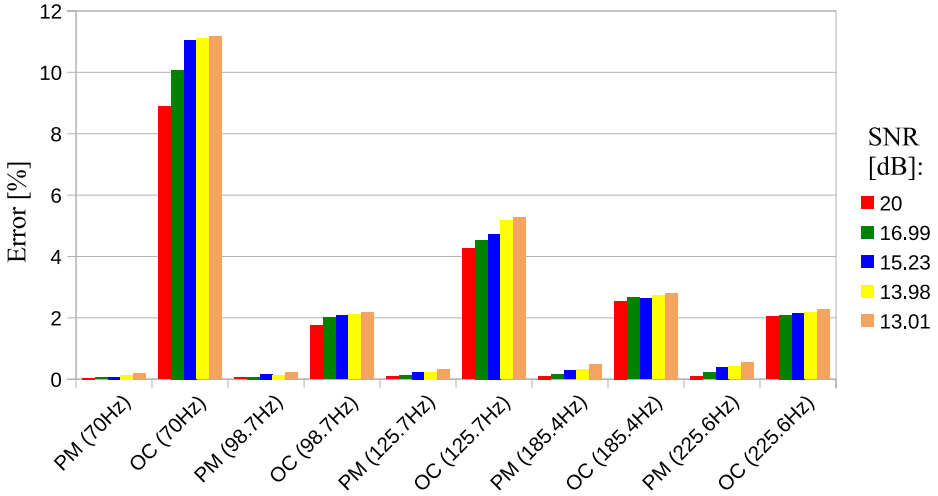

Fig. 8. Percentage estimation error of the phase angle ϕ of the fundamental component.

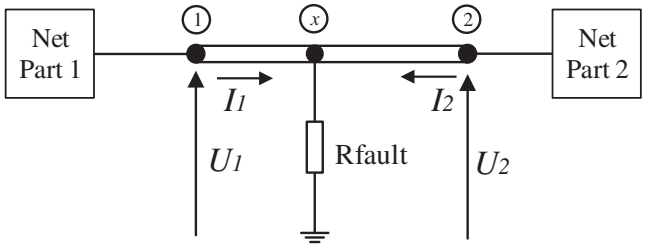

Fig. 9. Fault location in a transmission line.

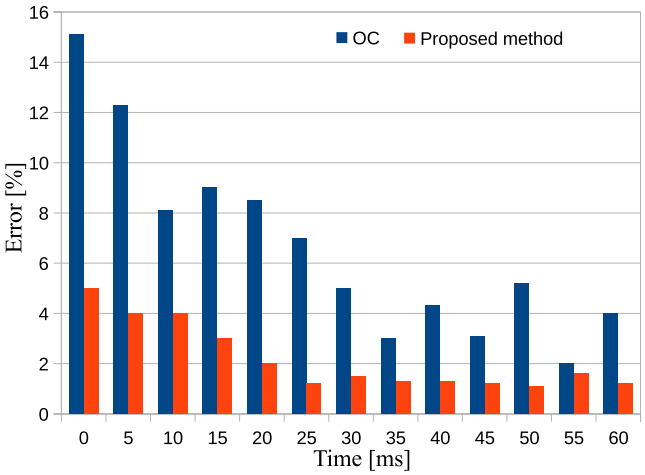

Fig. 10. Percentage error of the fault locator in [33] when phasors are extracted using the proposed method and the OC method.

4.1.1. Computational performance

Table 5 includes the minimum/average/maximum computational time and number of iterations for the nonlinear least-squares method; the statistics were obtained over 1000 Monte-Carlo simulations and recorded on a standard personal computer (i5-7600 K PC with 16 GB RAM). The results show that the nonlinear least-squares calculation requires no more than 235 ms and can require as low as 22 ms and one iteration; the number of iterations itself depends on the start point as computed by Kung's method. Kung's method is not iterative, and it consumes around 20 ms.

However, it is essential to note here that the computational time of the fault location method, including the fundamental frequency component extraction phase, is not a useful metric for comparison between competing methods; the main factor of concern is ultimately the accuracy of the fault location. In practice, fault location starts after the fault has already happened, and therefore a crew has to be sent to the actual fault location to fix the situation that caused the fault. Depending on where the fault has occurred, for instance, a mountain area with no road access, it may take several hours for the utility to have a specialized crew fixing the problem onsite. The time for fixing the fault would be even longer whenever the fault location is not accurately known. Therefore, finding an accurate location for the fault is the main requirement for having a timely solution for fault repair. The actual computational time of the fault location method is insignificant compared to the time for dispatching a team and repairing the fault. The nature of the fault location application, which is not a real-time function, makes the computational time comparison unimportant.

4.2. Simulation tests with frequency components having frequencies above 250 Hz

The decaying harmonics and inter-harmonics with frequencies above 250 Hz are not eliminated by the lowpass filter, but rather attenuated. The proposed method extracts the fundamental frequency component when some damped harmonics and inter-harmonics have their frequencies close to the fundamental frequency and are therefore not attenuated by the lowpass filter; this is the problematic case that motivated the development of the proposed method. Given that the proposed method can handle extracting the fundamental frequency component when the decaying harmonics and inter-harmonics have frequencies close to the fundamental frequency, the method can also surely operate when these components have frequencies much larger than the power system frequency.

To validate this point, additional testing was carried out on signals that have a fourth component, as shown in Table 6. The fourth component has a frequency that varies between 250 and 400 Hz in the Monte-Carlo trials, and its amplitude is around five times less than that of the first inter-harmonic, to simulate the output of a non-ideal lowpass filter. Table 7 shows the average relative error for both the PM and OC over 1000 Monte-Carlo trials; the relative errors for the extracted phasor amplitude and angle are reported in Table 7 at different values of SNR and f_{AC} and are also depicted graphically in Figs. 7 and 8. The figures clearly illustrate the superiority of the PM relative to OC; it is evident that the component that has the most impact on the OC method correctness has a frequency of 70 Hz, which is consistent with the frequency characteristic in Fig. 1. However, the inter-harmonic with a frequency of 98.7 Hz contributes to less error in the OC method, as this frequency is closer to the double of the fundamental frequency. The susceptibility of the OC method to the inter-harmonics is its major weakness as compared to the PM.

4.3. Simulation test with a real line

The proposed method for phasor extraction was employed in an implementation of the synchronized measurement technology-based fault locator [33]. A comparison was carried out using the same fault locator, but with the phasors extracted using the OC method in Section 2.1. The study aims to show the effect of phasor extraction using the proposed method and the OC method on a fault location methodology based on phasors. The simulation line data is from the Bosnian transmission network for the connection: Sarajevo 10 – Tuzla 4. The line data is: nominal voltage = 400 kV, conductor type = Al/Fe 490/65, length = 87.2 km, positive sequence line parameters (R = 2.7680 Ω, X = 28.0160 Ω, Bc = 0.984057 μF, Bg = 308.99 μS), and zero sequence parameters (R0 = 25.34 Ω,X0 = 74.14 Ω). The fault is simulated at 45 km from the left side in Fig. 9 with a fault resistance of 10 Ω, the SNR is at 20 dB, and the A/D converter has 16 bits.

The results in Fig. 10 show the percentage error in the fault distance as obtained from an implementation of [33] with the two phasor extraction methods. The error values are reported for different times of initiating fault location, varying between Time = 0, which is the fault inception time, and Time = 60 ms. At each time instant in Fig. 10, the data from the next full cycle (20 ms) is employed for the phasor extraction; for instance, at Time = 10 ms, only the signal data between 10 and 30 ms is employed for computing the phasors used in fault location. The results in Fig. 10 show that the proposed method results in less error than the OC method, and it also reveals that Kung's method most significantly improves fault location from cycles close to the very first moment of fault inception.

5. Conclusion

This paper presented an algorithm for the extraction of the fundamental frequency component from the measured voltage and current signals during a fault event. The algorithm is based on Kung's method to determine the initial modal information, followed by post-processing via nonlinear least-squares estimation. The proposed method is compared with a Fourier-based algorithm, which is the most practically used in protection relaying applications. The results show that the proposed method is more accurate than the Fourier-based algorithm,

and therefore gives phasor estimates that are more suitable for fault location. The effectiveness of the proposed method has been evaluated on simulated signals, and also when employed in a synchronized measurement technology-based fault locator.

Declaration of Competing Interest

The authors declare that they have no known competing financial interests or personal relationships that could have appeared to influence the work reported in this paper.

References

[1] Qi L, Woodruff S, Qian L, Cartes D. Time-varying waveform distortions in power systems. Wiley Blackwell; 2009 chapter 25: Prony analysis for time-varying harmonics. p. 383–400.
[2] He J, Liu J, Hao X, Wang X, Zhang X. Study on inter-harmonics in short-circuit current of hybrid AC/DC electric power systems. 2016 China international conference on electricity distribution (CICED). 2016. p. 1–5.
[3] Abdel-Fattah MF, Lehtonen M. Transient-based protection as a solution for earth-fault detection in unearthed and compensated neutral medium voltage distribution networks. Proceedings of the 2010 electric power quality and supply reliability conference. 2010. p. 221–8.
[4] Philippot L. Parameter estimation and error estimation for line fault location and distance protection in power transmission systems [Ph.D. dissertation]. Université Libre de Bruxelles; Feb. 1996.
[5] Saha MM, Izykowski J, Rosolowski E. Fault location on power networks. Springer-Verlag London Limited; 2010.
[6] Kezunovic M, Perunicic B. Synchronized sampling improves fault location. IEEE Comp Appl Power 1995;8(2):30–3.
[7] Izykowski J, Molag R, Rosolowski E, Saha MM. Accurate location of faults on power transmission lines with use of two-end unsynchronized measurements. IEEE Trans Power Deliv 2006;21(2):627–33.
[8] Benmouyal G. Removal of DC-offset in current waveforms using digital mimic filtering. IEEE Trans Power Deliv 1995;10(2):621–30.
[9] Yu C-S. A discrete Fourier transform-based adaptive mimic phasor estimator for distance relaying applications. IEEE Trans Power Deliv 2006;21(4):1836–46.
[10] Rosolowski E, Izykowski J, Kasztenny B. Adaptive measuring algorithm suppressing a decaying DC component for digital protective relays. Elec Power Syst Res 2001;60(2):99–105.
[11] Guo Y, Kezunovic M, Chen D. Simplified algorithms for removal of the effect of exponentially decaying DC-offset on the Fourier algorithm. IEEE Trans Power Deliv Jul. 2003;18(3):711–7.
[12] Yu C-S, Chen W-H. Removing decaying DC component in fault currents via a new modify discrete Fourier algorithm. IEEE power engineering society general meeting, vol. 1. 2005. p. 728–33.
[13] Kang SH, Lee DG, Nam SR, Crossley PA, Kang YC. Fourier transform-based modified phasor estimation method immune to the effect of the DC offsets. IEEE Trans Power Deliv 2009;24(3):1104–11.
[14] Silva KM, Nascimento FAO. Modified DFT-based phasor estimation algorithms for numerical relaying applications. IEEE Trans Power Deliv 2018;33(3):1165–73.
[15] Ren J, Kezunovic M. A hybrid method for power system frequency estimation. IEEE Trans Power Deliv 2012;27(3):1252–9.
[16] Lotfifard S, Faiz J, Kezunovic M. Detection of symmetrical faults by distance relays during power swings. IEEE Trans Power Deliv 2010;25(1):81–7.
[17] Rubeena R, Zadeh MRD, Bains TPS. An accurate offline phasor estimation for fault location in series-compensated lines. IEEE Trans Power Deliv 2014;29(2):876–83.
[18] Hauer JF, Demeure CJ, Scharf LL. Initial results in Prony analysis of power system response signals. IEEE Trans Power Syst 1990;5(1):80–9.
[19] de la O Serna JA. Synchrophasor estimation using Prony's method. IEEE Trans Inst Meas 2013;62(8):2119–28.
[20] Zhou N, Pierre J, Trudnowski D. Some considerations in using Prony analysis to estimate electromechanical modes. IEEE power energy society general meeting. 2013. p. 1–5.
[21] Kulp RW. "An optimum sampling procedure for use with the Prony method. IEEE Trans Electromag Compatibility 1981;EMC-23(2):67–71.
[22] Lee J-H, Kim H-T. Selecting sampling interval of transient response for the improved Prony method. IEEE Trans Antennas Propag 2003;51(1):74–7.
[23] Peng JC-H, Nair N-KC. Adaptive sampling scheme for monitoring oscillations using Prony analysis. IET Gener Transm Distrib 2009;3(12):1052–60.
[24] Ren J, Kezunovic M. Real-time power system frequency and phasors estimation using recursive wavelet transform. IEEE Trans Power Deliv 2011;26(3):1392–402.
[25] Ren J, Kezunovic M. An adaptive phasor estimator for power system waveforms containing transients. IEEE Trans Power Deliv 2012;27(2):735–45.
[26] Kung SY, Arun KS, Rao DVB. State-space and singular-value decomposition-based approximation methods for the harmonic retrieval problem. J Opt Soc Am 1983;73(12):1799–811.
[27] Hokanson JM. Numerically stable and statistically efficient algorithms for large scale exponential fitting [Ph.D. dissertation]. Houston, Texas: Rice University; Aug. 2013.
[28] Vandevoorde D. A fast exponential decomposition algorithm and its applications to structured matrices [Ph.D. dissertation]. Troy, New York: Rensselaer Polytechnic Institute; 1996.
[29] Dologlou I, Huffel SV, Ormondt DV. Frequency-selective MRS data quantification with frequency prior knowledge. J Mag Reson 1998;130(2):238–43.
[30] Luk FT, Qiao S, Vandervoorde D. Mathematics in Signal Processing V. ch. Exponential Decomposition and Hankel Matrix. Oxford University Press; 2002. p. 275–85.
[31] Tufts D, Kumaresan R. Singular value decomposition and improved frequency estimation using linear prediction. IEEE Trans Acoust Speech Signal Process 1982;30(4).
[32] Gratton S, Lawless A, Nichols N. Approximate Gauss-Newton methods for nonlinear least squares problems. SIAM J Optim 2007;18(1):106–32.
[33] Terzija V, Radojević ZM, Preston G. Flexible synchronized measurement technology-based fault locator. IEEE Trans Smart Grid 2015;6(2):866–73.
[34] Pham DM, Premkumar AB, Madhukumar AS. A/D conversion based on signal decomposition for DSP applications. IET 3rd international conference on wireless, mobile and multimedia networks (ICWMNN 2010), Sep. 2010. 2010. p. 44–7.
[35] IEEE standard for terminology and test methods for analog-to-digital converters. IEEE Std 1241-2010 (Revision of IEEE Std 1241-2000); Jan. 2011. p. 1–139.
[36] Sidhu TS, Zhang X, Balamourougan V. A new half-cycle phasor estimation algorithm. IEEE Trans Power Deliv 2005;20(2):1299–305.
[37] Wang L, Suonan J. A fast algorithm to estimate phasor in power systems. IEEE Trans Power Deliv 2017;32(3):1147–56.
[38] Zygarlicki J, Mroczka J. Pronys method used for testing harmonics and inter-harmonics in electrical power systems. Metrol Meas Syst 2012;XIX(4):659–72.
[39] Rahman MD, Yu K-B. Total least squares approach for frequency estimation using linear prediction. IEEE Trans Acoust Speech Signal Process 1987;35(10):1440–54.
[40] Boley DL, Luk FT, Vandevoorde D. Vandermonde factorization of a Hankel matrix. Proceedings of the workshop on scientific computing - Hong Kong. 1997.
[41] Chen H, Huffel SV, van Ormondt D, de Beer R. Parameter estimation with prior knowledge of known signal poles for the quantification of NMR spectroscopy data in the time domain. J Reson Ser A 1996;119(2):225–34.
[42] Vanhuffel S, Chen H, Decanniere C, Vanhecke P. Algorithm for time-domain NMR data fitting based on total least squares. J Mag Reson Ser A 1994;110(2):228–37.
[43] Barkhuijsen H, de Beer R, van Ormondt D. Improved algorithm for noniterative time-domain model fitting to exponentially damped magnetic resonance signals. J Mag Reson 1969;73(3):553–7. 1987.